A Novel Variable Stiffness Compliant Robotic Link Based on Discrete Variable Stiffness Units for Safe Human–Robot Interaction

Jiaming Fu

Polytechnic Institute, Purdue University, West Lafayette, IN 47907 e-mail: fu330@purdue.edu

Ziqing Yu

Polytechnic Institute, Purdue University, West Lafayette, IN 47907 e-mail: yu1154@purdue.edu

Han Lin

Polytechnic Institute, Purdue University, West Lafayette, IN 47907 e-mail: lin853@purdue.edu

Lianxi Zheng

Professor Department of Mechanical Engineering, Khalifa University of Science and Technology, P. O. Box 127788, Abu Dhabi, UAE e-mail: lianxi.zheng@ku.ac.ae

Dongming Gan¹

Assistant Professor Mem. ASME Polytechnic Institute, Purdue University, West Lafayette, IN 47907 e-mail: dgan@purdue.edu

Variable stiffness manipulators balance the trade-off between manipulation performance needing high stiffness and safe human-robot interaction desiring low stiffness. Variable stiffness links enable this flexible manipulation function during humanrobot interaction. In this paper, we propose a novel variable stiffness link based on discrete variable stiffness units (DSUs). A DSU is a parallel guided beam that can adjust stiffness discretely by changing the cross-sectional area properties of the hollow beam segments. The variable stiffness link (Tri-DSU) consists of three tandem DSUs to achieve eight stiffness modes and a stiffness ratio of 31. To optimize the design, stiffness analysis of the DSU and Tri-DSU under various configurations and forces was performed by a derived linear analytical model which applies to small/intermediate deflections. The model is derived using the approach of serially connected beams and superposition combinations. 3D-Printed prototypes were built to verify the feature and performance of the

Tri-DSU in comparison with the finite element analysis and analytical model results. It's demonstrated that our model can accurately predict the stiffnesses of the DSU and Tri-DSU within a certain range of parameters. Impact tests were also conducted to validate the performance of the Tri-DSU. The developed method and analytical model are extendable to multiple DSUs with parameter configurations to achieve modularization and customization, and also provide a tool for the design of reconfigurable collaborative robot (cobot) manipulators. [DOI: 10.1115/1.4056957]

Keywords: compliant mechanisms, mechanism design, robot design

1 Introduction

Due to technical reasons, humans are excluded from the work area to ensure safety during traditional industrial robot work [1]. For example, the welding process in the automobile manufacturing process does not require human participation at all, and safety fences are used to separate workers and robots [2]. However, many jobs require human participation that cannot be automated to a high degree by robots so far [3]. As a result, a cobot, a type of robot that can safely interact directly with operators, is growing at a rapid pace [4]. In manufacturing, the introduction of collaborative robots can make full use of the efficiency of robots to compensate for the low human precision, strength, and durability, while retaining human intelligence and skills [5].

Researchers have explored from the perspective of materials, using soft materials to make robotic arms to reduce impact forces during collisions. In Ref. [6], the arm was wrapped with pneumatic artificial muscles and inflatable sleeves. In Ref. [7], a soft robotic arm driven by shape memory alloy (SMA) coils was reported. In Ref. [8], a soft robotic arm (SRA) made from nylon fabric was proposed. However, while low stiffness brings safe interaction, it compromises performance on accuracy and payload which needs high stiffness. This has led to variable stiffness manipulators to balance the two sides.

To enable variable stiffness compliant manipulation, researchers innovate from the perspective of mechanical design by adding variable stiffness actuators (VSA) to the robot joints to achieve safe interaction. Some VSAs are based on the variable impedance actuation (VIA) method to increase the torque bandwidth and reduce structure sizes [9–12]. In Refs. [13,14], the VSAs are able to adjust stiffness by changing the effective beam length to achieve continuous variable stiffness. In Refs. [15,16], the VSAs can achieve discrete variable stiffness.

Another method for developing variable-stiffness-compliant manipulators is to design variable stiffness links. A variable stiffness robotic arm based on a rotating beam link was proved to be feasible [17,18] and other manipulators based on compliant parallel guide beams were also developed [19–21]. The compliant link can produce less impact force in collisions than a compliant joint [22], in cases where the arm mass is greater than the end-effector mass. However, compared to VSAs and compliant end effectors [23–25], little research has been done on compliant robotic links. Therefore, it is necessary to expand the research in this field.

The majority of published variable stiffness robotic links are continuous variable stiffness, but there are many cases where continuous adjustment is not necessary. Inspired by our previous work on discrete variable stiffness actuators [26,27], the design of a compact discrete variable stiffness robot link with fast stiffness change and a large stiffness change ratio provides a more practical development direction. We proposed a reconfigurable variable stiffness parallel beam (VSPB) [28] and develop a discrete variable stiffness unit (DSU) in this work, which achieves discrete variable stiffness by changing the cross-sectional area property. The main structure of the DSU is a parallel guided beam that can adjust stiffness by a push–pull solid block to the cavity of the beam. The solid block is mounted on the stroke of a linear actuator, which is fixed to the side of the solid body of the DSU near the pedestal end of the

¹Corresponding author.

Contributed by the Mechanisms and Robotics Committee of ASME for publication in the JOURNAL OF MECHANISMS AND ROBOTICS. Manuscript received October 15, 2022; final manuscript received February 8, 2023; published online March 8, 2023. Assoc. Editor: Guimin Chen.

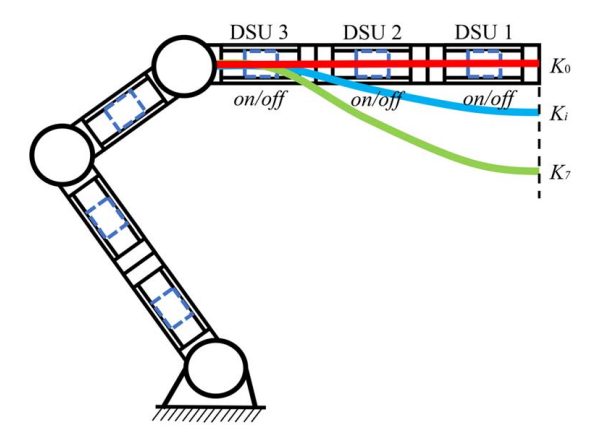


Fig. 1 Cobot with variable stiffness links

robotic arm. The variable stiffness robotic link (Tri-DSU) consists of three tandem DSUs, each of which can be adjusted individually to achieve a total of eight stiffness modes, as shown in Fig. 1.

Compared with existing compliant links, the Tri-DSU has the following main advantages: (1) It has a simple and compact structure because of using mini-size linear actuators to drive the blocks; (2) It has low energy consumption because the linear actuator module operates on very low power and is energized only when the system is switching stiffness modes. (3) It provides fast stiffness change as the linear actuator module is activated in an on/off manner to complete the variable stiffness task, which improves the efficiency of the system. We also derive accurate linear analytical models for DSU and Tri-DSU within a certain range of parameters, which applies to small/intermediate deflections (within 10% of the beam length). Our models do not require experimental determination of coefficients for new designs as compared to the pseudo-rigid body (PRB) model [29,30].

The paper is organized as follows: Sec. 2 introduces the mechanical design and concept implemented for the stiffness variation of Tri-DSU; Sec. 3 develops the analytical model of the stiffness variation; Sec. 4 describes finite element analysis (FEA) simulation and experimental validation; Sec. 5 compares the analytical model, FEA, and experimental values; Sec. 6 conducts the impact test; Sec. 7 concludes the work.

2 Mechanical Design

2.1 Working Principle of Stiffness Variation. As shown in Fig. 2, the Tri-DSU is a variable stiffness link consisting of three serial-connected DSUs. Figure 3 illustrates the main structure of the DSU, which is a parallel guided beam that can adjust stiffness discretely by a push-pull solid block to the cavity of the beam. The on/off mode of the block changes the second area of the

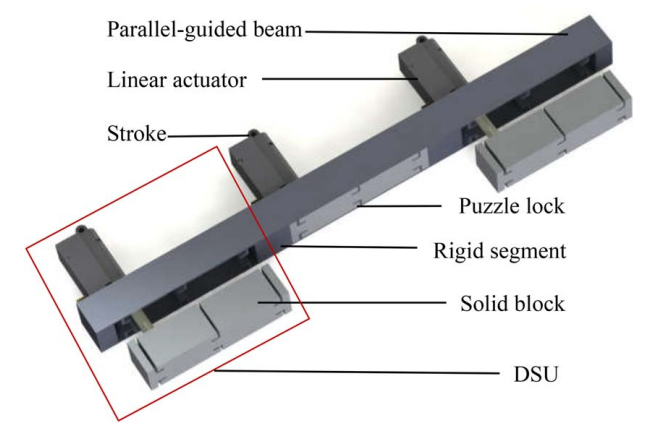


Fig. 2 The stiffness change principle of Tri-DSU

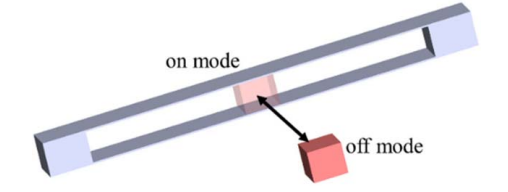


Fig. 3 The stiffness change principle of DSU

moment of inertia of the beam leading to stiffness varying. The illustrated DSU design is 3D-printed with polylactic acid (PLA) with dimensions $100 \times 18 \times 20$ mm. The length of the cavity is 80 mm, and the thickness of the parallel beams is 1 mm. A linear actuator is fixed to the solid segment on the side of the DSU near the pedestal end of the arm to reduce the impact on the flexible structure of the DSU because the solid segment has almost no deformation. The model of the compact linear actuator is ACTUONIX PQ12-P with a 20-mm stroke. The solid block is mounted on the stroke of the linear actuator, and the stroke passes through the cavity near the solid segment. When the parallel beam bends, the deformation of the middle part of the beam is large and the deformation of the ends is small, relatively. Therefore, the stroke does not contact the beam and does not interfere with the deformation of the beam. When the stroke is extruded, the solid block is pushed out of the cavity of the parallel beam, called off mode; now, the DSU has relatively low stiffness and high compliance. When the stroke is retracted, the solid block is pulled into the cavity, called on mode, where the DSU has relatively high stiffness and accuracy. The extrusion or retraction process of the stroke takes only 0.2 s, which means that the DSU can change its stiffness rapidly. When the beam has a large deformation, the block cannot be inserted or pushed out smoothly, so the DSU can only achieve offline variable stiffness, which still covers most of the application scenarios.

2.2 Stiffness Configurations. An individual DSU may not achieve the desired deflection, therefore, multiple DSUs can be considered to be connected in series to increase compliance. The Tri-DSU consists of three DSUs connected in series, so each DSU can be adjusted individually to achieve the eight stiffness modes of the entire system. When all DSUs are in off mode, the Tri-DSU is in off-off-off (FFF) mode, and the system has the lowest stiffness. When two DSUs are in off mode and another DSU is in on mode, the Tri-DSU may be in off-off-on (FFN) mode, off-on-off (FNF) mode, or on-off-off (NFF) mode. In these three cases, the stiffness of the Tri-DSU is relatively low and close to each other, only the position of the flexible segment is different. When two DSUs are in on mode and the other two DSUs are in off mode, the Tri-DSU may be in on-on-off (NNF) mode, on-off-on (NFN) mode, or off-on-on (FNN) mode. In these three cases, the stiffness of Tri-DSUs is relatively high. When all DSUs are in on mode, the Tri-DSU is in on-on-on (NNN) mode, and the system has the largest stiffness. Theoretically, the Tri-DSU in such a parameter configuration can achieve a stiffness ratio of 57.

The design of the DSU can be modular and customizable. The dimensions and materials of the prototypes are only examples and can be adapted to various requirements, or more DSUs can be connected in series to construct multiple DSU structures. In a DSU, the hollow parallel beam part in the middle and the solid rigid parts at both ends also have a certain thickness rather than being treated as thin walls [31,32]. In order to systematically elaborate the variable stiffness principle of DSUs, a generalized stiffness modeling approach is developed to lay the theoretical foundation for further design and application of this novel variable stiffness mechanism.

3 Stiffness Modeling

3.1 Analytical Stiffness Model of the Discrete Variable Stiffness Unit. Figure 4 illustrates the basic geometry structure

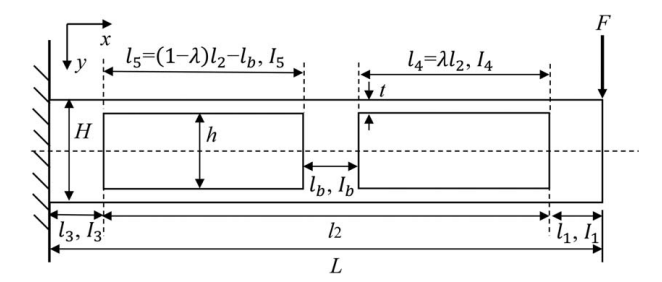


Fig. 4 Free body diagram of DSU

of a DSU. The total length of the parallel guided beam with a block inside is L in an x-y coordinate system: the x-axis direction is horizontal along the long axis of the beam to the right, and the y-axis is perpendicular to the x-axis and downward while the z-axis is ignored since the beam is considered only working on the x-y plane.

Assuming that the left end of the beam is fixed to the wall, downward force F acts perpendicular to the x-axis and is applied to the right end of the beam. One of the main characteristics of the parallel guide beam is that the load end does not rotate under loading, unlike the cantilever beam at the free end. In the range of small and intermediate deflections, the contribution of rotation of cross sections to axial strain is very small. In this case, its geometric nonlinearity can be neglected. Therefore, the axial load and parasitic displacement [33] at the load end are too small that they can be omitted compared with the values in the y-direction. Most deflection of the beam will be generated by the compliant segments, which are l_4 and l_5 , but solid segments of l_1 , l_b , and l_3 should not be ignored because they have a certain deformation in real applications and their elasticity will affect the accuracy of the model when their length is longer than the compliant segments. The stiffness of the DSU is adjustable by the block in the cavity. When the DSU is in the off mode, l_b is equal to zero, and if the DSU is switched to on mode, l_b will be greater than zero and no bigger than l_2 .

The beam is divided into five segments in this case, where l_1 , l_b , and l_3 are solid bodies with the moment of inertia I_1 , I_b , and I_3 , respectively. The segments l_4 and l_5 are parallel beams with the moment of inertia I_4 and I_5 . The length of l_2 is equal to the sum of l_4 , l_b , and l_5 . To facilitate calculation and analysis, the l_4 is parameterized as λl_2 . Thus, l_5 is equal to $(1-\lambda)$ $l_2_l_b$. To get an accurate result, the deflections of the beam are computed segment-by-segment and then superpose the results together. The calculation process of the deflection and stiffness of the DSU is shown below.

The height of the DSU is H, and the height of the cavity is h. Thus, the thickness of the leaf springs in l_4 and l_5 is t = (H - h)/2. The width of the beam, b, is perpendicular to the surface of the paper but not marked in Fig. 4, which. Then the moment of inertia of each segment can be obtained:

$$I_1 = I_3 = I_b = \frac{H^3 b}{12} \tag{1}$$

$$I_4 = I_5 = \frac{t^3 b}{12} \tag{2}$$

First, segments l_2 and l_3 are considered rigid, and only segment l_1 is compliant. Thus, the deflection δ_1 at the end of l_1 can be calculated by the normal cantilever beam equation, where E is Young's modulus of the DSU

$$\delta_1 = \frac{Fl_1^3}{3EI_1} \tag{3}$$

Next, the other parts are treated as rigid bodies and only segment l_4 is compliant. In addition to the forces that cause a deflection angle and deflection to l_4 , the bending moment from l_1 also causes a deflection angle and deflection to L. Based on the theory of parallel guided mechanism [34], then, the following are derived formulas to

calculate the total deflection angle θ_2 and total deflection δ_2 of the compliant segment l_4 under both force and moment:

$$\theta_2 = \frac{t^2}{6h^2} \left(\frac{Fl_1(\lambda l_2)}{EI_4} + \frac{F(\lambda l_2)^2}{2EI_4} \right) \tag{4}$$

$$\delta_2 = \frac{F(\lambda l_2)^3}{24EI_4} + \frac{t^2}{12h^2} \left(\frac{Fl_1(\lambda l_2)^2}{EI_4} + \frac{F(\lambda l_2)^3}{2EI_4} \right)$$
 (5)

Similarly, the other segments are treated as rigid bodies to calculate the deflection angle θ_3 and deflection δ_3 of segment l_b

$$\theta_3 = \frac{Fl_b^2}{2EI_b} + \frac{F(l_1 + \lambda l_2)l_b}{EI_b}$$
 (6)

$$\delta_3 = \frac{Fl_b^3}{3EI_b} + \frac{F(l_1 + \lambda l_2)l_b^2}{2EI_b} \tag{7}$$

The deflection angle θ_4 and deflection δ_4 of the compliant segment l_5 are

$$\theta_4 = \frac{t^2}{6h^2} \left(\frac{F(l_1 + \lambda l_2 + l_b)[(1 - \lambda)l_2 - l_b]}{EI_5} + \frac{F[(1 - \lambda)l_2 - l_b]^2}{2EI_5} \right)$$
(8)

$$\delta_4 = \frac{F[(1-\lambda)l_2 - l_b]^3}{24EI_5} + \frac{t^2}{12h^2} \left(\frac{F(l_1 + \lambda l_2 + l_b)[(1-\lambda)l_2 - l_b]^2}{EI_5} + \frac{F[(1-\lambda)l_2 - l_b]^3}{2EI_5} \right)$$
(9)

To compute the deflection angle θ_5 and deflection δ_5 of segment l_2 as below:

$$\theta_5 = \frac{Fl_3^2}{2EI_3} + \frac{F(l_1 + l_2)l_3}{EI_3} \tag{10}$$

$$\delta_5 = \frac{Fl_3^3}{3EI_3} + \frac{F(l_1 + l_2)l_3^2}{2EI_3} \tag{11}$$

Finally, all the deflection acting on the end of the DSU are accumulated to get its maximum deflection δ_A and the stiffness k_A can be calculated using Eqs. (12) and (13)

$$\delta_A = \delta_1 + \delta_2 + \delta_3 + \delta_4 + \delta_5 + \theta_2 l_1 + \theta_3 (l_1 + \lambda l_2) + \theta_4 (l_1 + \lambda l_2 + l_b) + \theta_5 (l_1 + l_2)$$
(12)

$$k_A = \frac{F}{\delta_A} \tag{13}$$

3.2 Analytical Stiffness Model of the Tri-Discrete Variable Stiffness Unit. As illustrated in Fig. 5, the Tri-DSU consists of three DSUs connected in series. To achieve modularity and customization, we develop an analytical stiffness model for the Tri-DSU

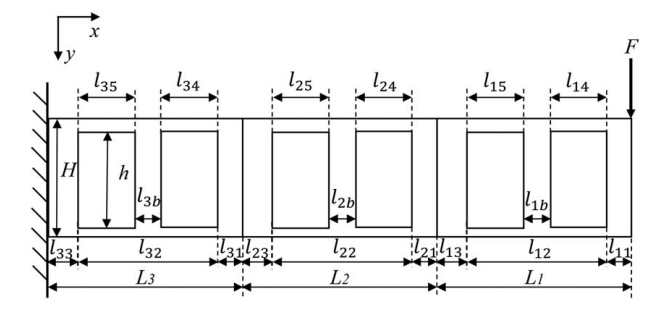


Fig. 5 Free body diagram of the Tri-DSU

that is also adaptable to multi-DSU designs. The method is based on the model in Sec. 3.1 for single DSUs with the same force conditions and coordinate system.

In the case of Tri-DSU, l_{ij} represents the jth segment in the ith DSU from the free end to the fixed end. Therefore, the Tri-DSU is divided into 15 segments, from l_{11} to l_{33} . We can compute the deflections δ_A , δ_B , and δ_C of segments L_1 , L_2 , and L_3 respectively. Then, the total deflection δ_{total} that acts on the end of the Tri-DSU can be calculated by accumulating the deflection of all three DSUs using Eq. (14)

$$\delta_{total} = \delta_A + \delta_B + \delta_C \tag{14}$$

4 FEA Simulation and Experimental Validation

- **4.1 Construction of the Prototype.** Based on the design and concept in Sec. 2, a Tri-DSU prototype was constructed by 3-D printing. PLA was chosen as the primary material due to its high toughness and strength characteristics. The design of the Tri-DSU was simplified during the construction of the prototype. The three DSUs were printed directly as a single body. Linear actuators were not used, but rather the on and off of the solid blocks were implemented manually. The material of prototypes was filled with 40%, and the layer height was 0.2 mm in 3-D printing.
- 4.2 Determination of Material Properties. The mechanical properties of the same material with various printing parameters are different. The properties of PLA are not provided at 40% filament, such as density, Young's modulus (E), and Poisson's ratio. Young's modulus was measured accordingly to its definition, i.e., the longitudinal stress divided by the strain. However, the results obtained were significantly smaller than the theoretical values. One reason could be that the 3D-printed parts are anisotropic due to the different patterns and fills during printing. Thus, using the deflection formula for the cantilever beam could find more accurate values of E than based on its definition. Then, we measured the force and deflection to calculate E by using Eq. (3), which is 3472 MPa. To make the results as accurate as possible, a cantilever beam with similar dimensions to one DSU was used with the same print configuration of the whole Tri-DSU, being $100 \times 18 \times 1$ mm. Moreover, we measured the density of PLA at 40% filling and 0.2-mm profiles to be 0.78 g/cm³. Also, the Poisson's ratio was determined to be 0.35, according to the negative ratio of the transverse strain to the axial strain.
- 4.3 Finite Element Analysis Simulation. To verify the accuracy of the analytical model in Sec. 3 and to find the optimal parameters of the DSU, we control the variables and define the width of the beam b, the length of the parallel beam segment l_2 , and its thickness t as the independent variables in the off mode, and in addition, for the on mode, the scaling factor λ of the length of the l_4 segment and the length of the solid block l_b are also considered. For each independent variable, ten models with different parameters were set. FEA simulations were performed on these models to analyze the static forces under various force scenarios. In ANSYS, a customized PLA material was set up by using the parameters measured in Sec. 4.2. The simulation was also performed for eight configurations of the Tri-DSU, as described in Sec. 2. The parameters of the 3-D model used in the simulation are the same as those of the prototype used for the experiments. One end of the beam is fixed, and the other end is stressed along the Y-axis, which is similar to the force condition of a robotic arm in practical application. The large deflection switch is off. Figure 6 compares the deformation of the Tri-DSU between FEA at a scale of 1:1 and prototype test under FNF mode.
- **4.4 Experimental Validation.** To verify the accuracy of the FEA simulation, stiffness experiments on DSUs and Tri-DSUs

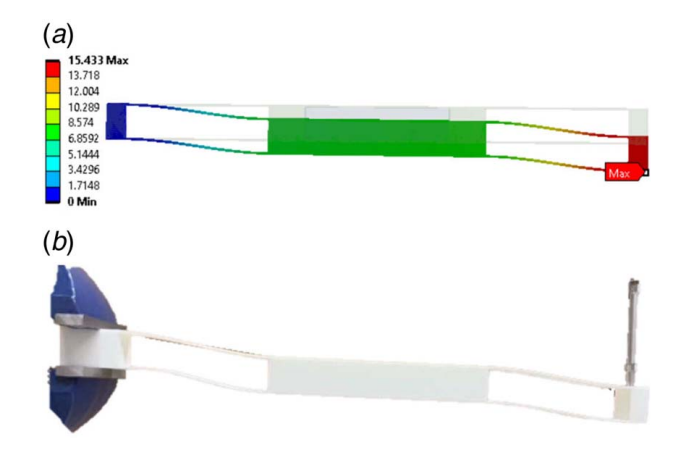


Fig. 6 Deformation of the Tri-DSU under FNF mode: (a) FEA and (b) prototype

were performed. As shown in Fig. 7, a 3D-printed Tri-DSU was mounted on a bench vise. A Mark-10 M5-100 force gauge was mounted on an ESM303 test stand to measure the force applied to the end of the beam. A probe with a flat tip was selected because it is the closest to the real load situation. The probe applies forces at the end of the 3D-printed link. The force and displacement are zeroed, which counteracts the effect of gravity on the link. Then, the force threshold is set, and the probe will automatically depress until the threshold is reached, which is the same as the setting in ANAYS. To reduce error, the experiment is repeated ten times for each model, and then, the results are averaged.

4.5 Puzzle Lock Mechanism. As shown in Fig. 8, we designed a puzzle lock mechanism for the DSU to limit the unexpected sliding of the solid block in the on mode on both the x-axis and y-axis. The L-shape beam of the puzzle lock is only 1 mm thick to reduce the effect on the parallel beam deformation as much as possible. As shown in Figs. 8(a) and 8(b), in the off mode, the stiffness of the DSU without puzzle lock is 0.065 N/mm, while the stiffness with puzzle lock is 0.066 N/mm. This indicates that in the off mode, the puzzle lock has almost no effect on the stiffness of the parallel beam. As shown in Figs. 8(c) and 8(d), in the on mode, the stiffness of the conjoined DSU is 1.32 N/mm in the case of integrated printing frame and block, while the stiffness with the puzzle lock is 1.24 N/mm, and the two stiffnesses are very close. However, as shown in Fig. 8(e), when the solid block is inserted into the cavity without puzzle

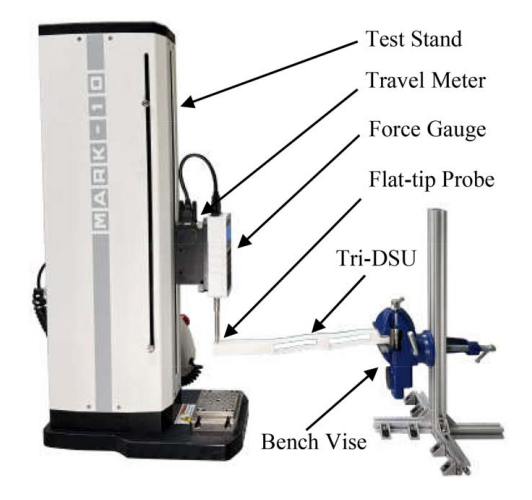


Fig. 7 The stiffness experiment setup

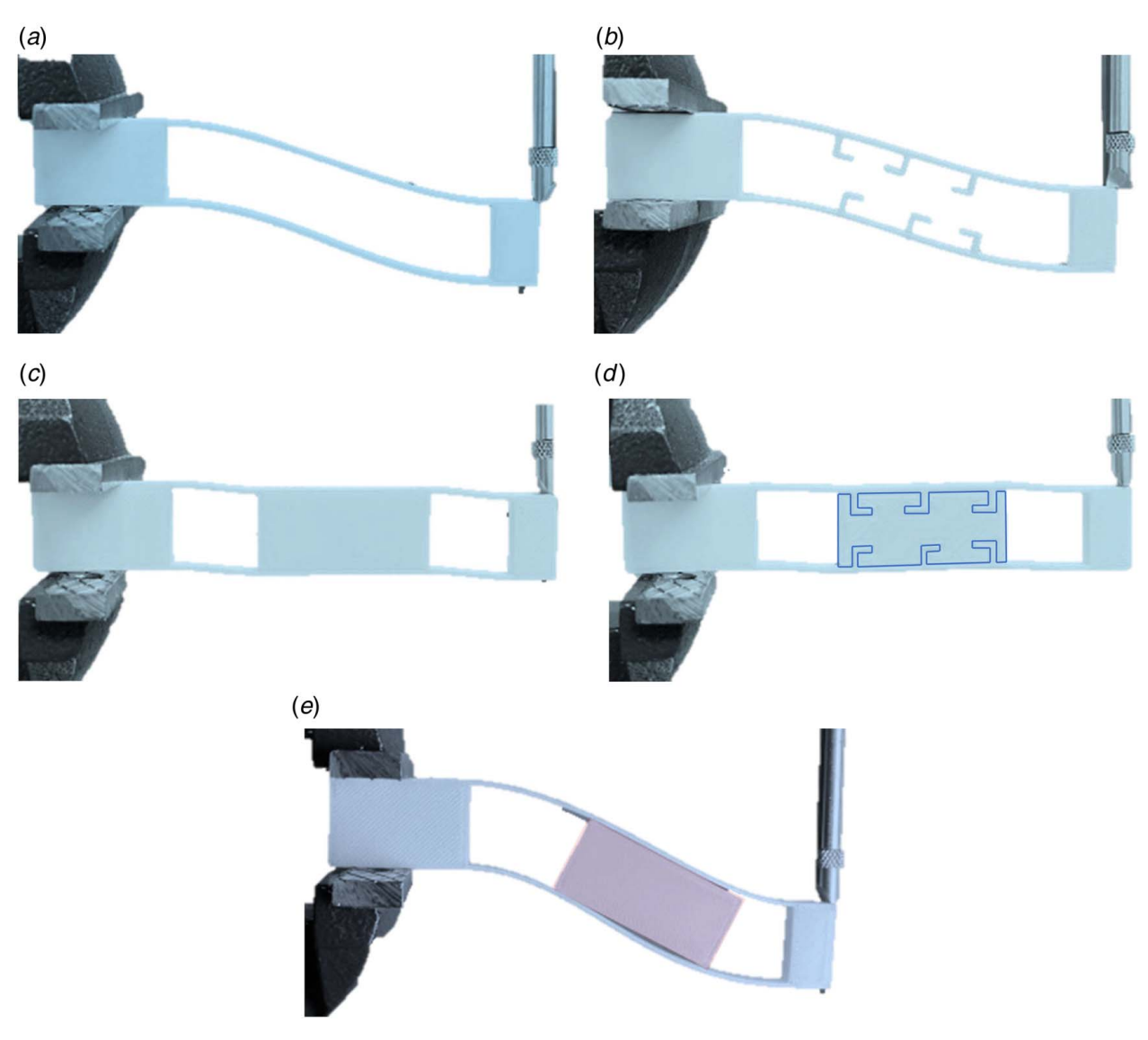


Fig. 8 Comparison of DSU with and without puzzle lock design: (a) normal DSU in off mode, (b) DSU with puzzle lock in off mode, (c) conjoined DSU in on mode, (d) DSU with puzzle lock in on mode, and (e) normal DSU (without puzzle lock) in on mode

lock constraint, it leads to a stiffness of $0.080\,\text{N/mm}$ only. Thus, the puzzle lock design can significantly solve the sliding problem of the solid block.

5 Results

5.1 Result Analysis of the Discrete Variable Stiffness Unit.

The deflection and stiffness data of DSUs with different parameters and configurations under various forces were collected by ANSYS simulations, MATLAB calculations by using our analytical model, and experiments. To facilitate the analysis and comparison, we standardized the available parameters, for example, using h/H to denote the thickness ratio of the leaf spring. A larger value of this ratio means that the thickness of the leaf spring is smaller, which will theoretically reduce the stiffness of the whole DSU. l_2/L represents the ratio of the length of the parallel beam. A larger value of l_2/L means a larger percentage of the compliant segment's length, which will also lead to low stiffness. b/L represents the width ratio of the DSU. A larger b/L means that the beam is wider and will provide a higher stiffness. λ reflects the change in the position of the solid block in the cavity. When λ approaches 0.5, this represents that the block is near the middle of the cavity, and therefore, the beam can obtain more stiffness. When λ tends to 0, it means that the block is near the end of the cavity, and therefore, the beam can obtain lower stiffness. l_b/L represents the percentage of the block for the whole beam length, which reflects the variation of the block size in the central region of the cavity. When the value of l_b/L rises, the stiffness of the DSU will increase. When l_b/L is 0, it represents that there is no solid block in the cavity, which is the off mode. When $l_b/L=1$, the DSU becomes a solid cantilever beam. The DSU model mentioned in Sec. 2 is used in the experiment and FEA, where all other parameters are kept constant when one parameter is investigated.

Figure 9(a) illustrates the relationship between h/H and the DSU stiffness, when the h/H ratio is less than 0.5, it means that the total thickness of the two parallel beams is more than half of the thickness of the whole beam, at this time, its mechanical properties are beyond the range of compliance. This uncommon range can be circumvented when designing variable stiffness links. However, when h/H is greater than 0.5, it is in the normal design range, where the errors between the analytical model and FEA are not exceeded 5%. When h/H is less than 0.7, the error between the experimental value and FEA becomes large. The most likely reason is that when the beam becomes thicker, the deformation of the entire DSU is less than 1 mm. In these situations, the numerical error is quite small, but the error in percentage measurement will be magnified. When h/H is greater than 0.7, the error of all three values is less than 10%. As shown in Fig. 9(b), when l_2/L is less than 0.2, the error

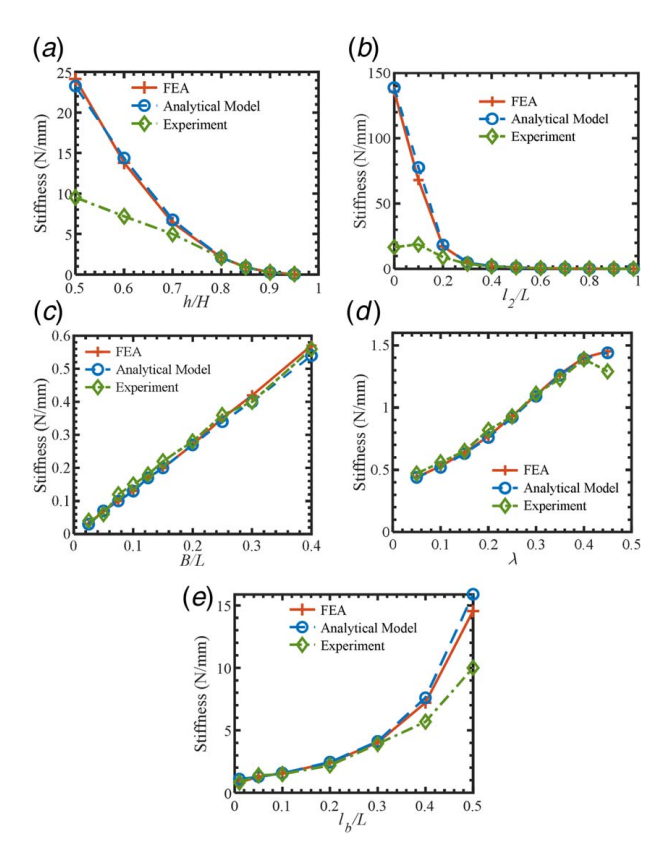


Fig. 9 Comparison of the stiffness of the DSU of FEA, theoretical value, and experimental value: (a) h/H versus stiffness, (b) I_2/L versus stiffness, (c) b/L versus stiffness, (d) λ VS stiffness, and (e) I_b/L VS stiffness

between FEA and the experimental value increases significantly, most likely for the same reason as in the case of h/H, while the error relative to the theoretical value and FEA is always within 5%. Figure 9(c) illustrates the relationship between b/L and the DSU stiffness which are generally proportional. In these cases, the errors in all of the theoretical and experimental values and FEA are less than 5%. Figure 9(d) shows the stiffness becomes larger with bigger λ . In these cases, the errors of all of the FEA, theoretical, and experimental values are less than 5% until $\lambda = 0.5$. As shown in Fig. 9(e), the stiffness increases when l_b/L increases, where the error between the FEA and the theoretical value is always less than 5%. However, when the value of l_b/L is greater than 0.5, the error between the FEA and the experimental value increases significantly, most likely for the same reason as in the case of h/H. Therefore, to achieve a more significant change in stiffness, it is better to make the length of the parallel beam in the DSU as long as possible, the thickness of the leaf spring as thin as possible, and the solid block as long as possible.

5.2 Result Analysis of the Tri-Discrete Variable Stiffness

Unit. Figure 10 shows the force and deflection relationships, i.e., stiffness relationships, of the Tri-DSU under eight stiffness configurations. For each configuration, the error between the FEA and the theoretical values is less than 3%. For all seven configurations except the NNN mode, the errors between FEA and experimental values are less than 20%. For NNN mode, the error between FEA and experimental values reaches 109%, which is because both of them have a deflection of less than 1 mm under the load of 2 N, so the error percentage is magnified. In fact, they have an error of only 0.4 mm. A better result could be achieved by using metallic materials without anisotropy such as aluminum or steel.

The minimum theoretical stiffness of the Tri-DSU is 0.09 N/mm in the FFF mode, while the maximum theoretical stiffness is

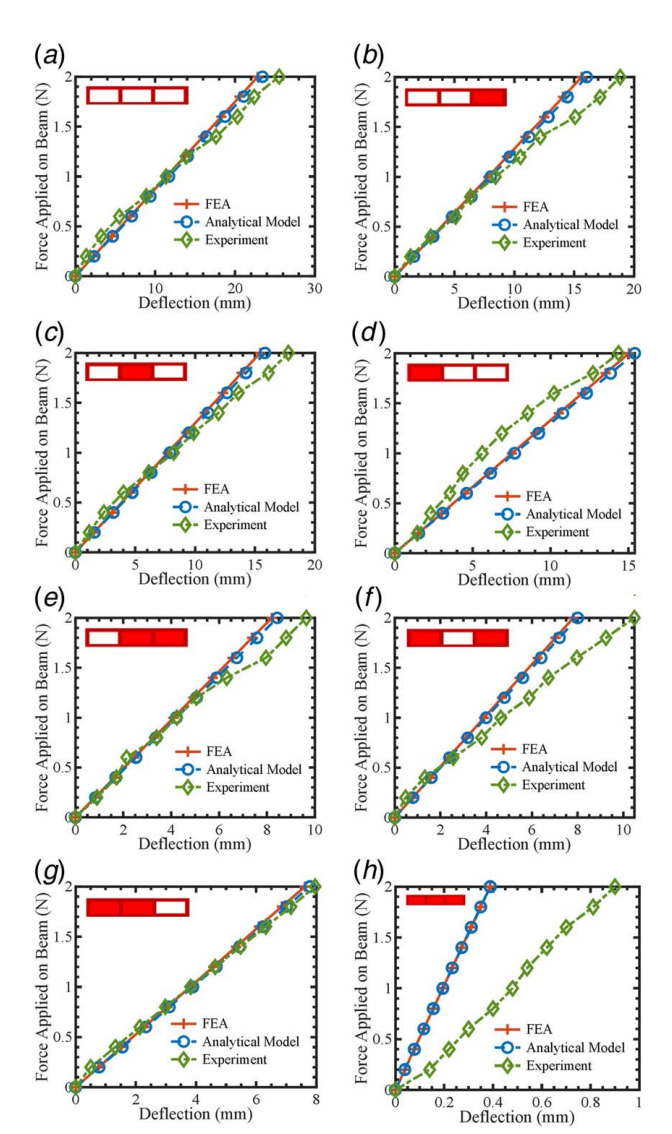


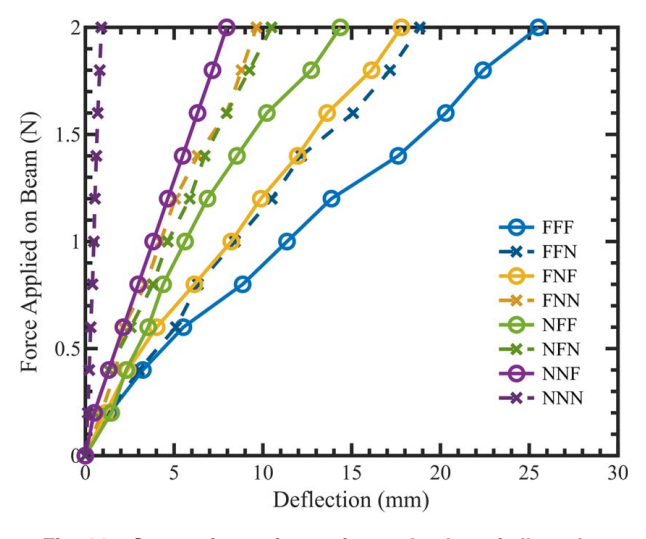
Fig. 10 Comparison of the stiffness of the Tri-DSU of FEA, theoretical value, and experimental value in different configurations: (a) FFF mode, (b) FFN mode, (c) FNF mode, (d) NFF mode, (e) FNN mode, (f) NFN mode, (g) NNF mode, and (h) NNN mode

5.16 N/mm when it is in the NNN mode. Thus, Tri-DSU can theoretically achieve a 57-fold change in stiffness. Figure 11 compares the experimental values of the eight configurations of the Tri-DSU, which are consistent with the design in Sec. 2. The FFN, FNF, and NFF modes have lower and similar stiffnesses, but different configurations. The FFN, NFN, and NNF modes have higher and similar stiffnesses. The FFF mode has the lowest stiffness with an experimental value of 0.08 N/mm, and the NNN mode has the highest stiffness with an experimental value of 2.47 N/mm. Thus, the Tri-DSU can actually achieve a 31-fold variation in stiffness based on the developed prototypes.

6 Experimental Impact Tests

After analyzing the stiffness of the Tri-DSU, a preliminary impact test of the Tri-DSU was conducted to verify the impact effect of different stiffness configurations. The impact tests measured and recorded the variations of impact forces at different velocities and stiffness configurations.

The experimental setup of the measurement of impact forces is shown in Fig. 12. Each DSU on the Tri-DSU has a linear actuator, which is individually controlled by a motor driver and a



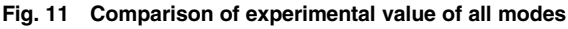




Fig. 12 Experiment setup of the impact test

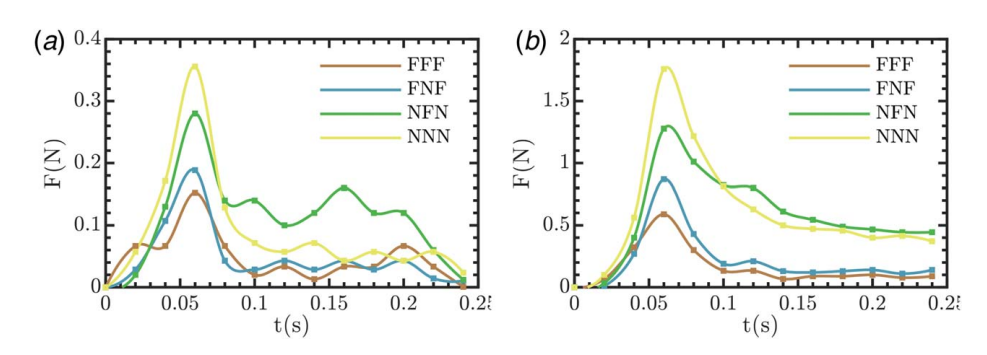


Fig. 13 Variation of impact force with time: (a) 0.5 m/s and (b) 1 m/s

microcontroller for extension and retraction. One end of the Tri-DSU is mounted on the base of the robot arm (LeArm) and driven by a servo motor, which allows angular velocity and angular position control. This enables the end of the Tri-DSU to impact the probe of the force gauge at different speeds. The force is recorded by the force gauge over time. The force measurement devices used here are the same as in the stiffness experiment but are placed horizontally.

The linear velocity of the end-effector of collaborative robots is typically within 1 m/s. Figure 13 shows the impact force versus time for the velocity of the Tri-DSU at 0.5 m/s and 1 m/s. Only four stiffness configurations are shown here because FNN, NFN, and NNF modes have similar stiffness levels; thus, NFN mode is selected. Similarly, when only one block is in the on mode, the FNF mode is selected. Compared with the NNN mode which has the highest stiffness, NFN mode can reduce the impact force by 27%, FNF mode can lower the force by 51%, and FFF mode can reduce the force by 67% during the test. When the collision occurs at 1 m/s, the peak impact forces for NNN mode and FFF mode are 1.76 N and 0.58 N, respectively. The relationship between the impact force and the velocity of the Tri-DSU is shown in Fig. 14 for the four different stiffness modes. The Tri-DSU has a peak impact force of 1.06 N under FFF mode at 2 m/s, and the corresponding deflection is 12.11 mm. It is only 4% of the total length (30 cm) of the Tri-DSU, which indicates that most of the impact scenarios are in the range of small to intermediate deflection for the Tri-DSU.

This preliminary experiment confirms that the low stiffness mode of the Tri-DSU can help to achieve safe human-robot interaction even at high speeds of cobots. However, the sampling frequency of the sensors in this experiment is still not high enough to make

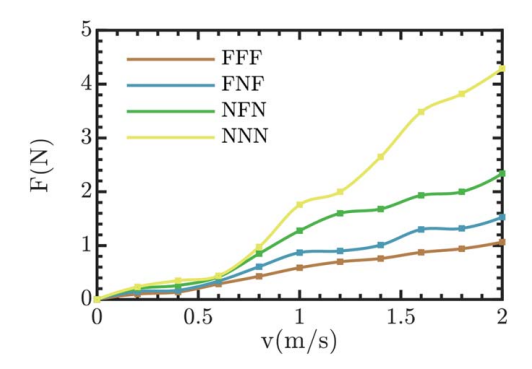


Fig. 14 Impact force at various velocities

the evaluation accurate. Multiple measurements were averaged to reduce the error. Due to the limited density and strength of the 3D printing material, the weight of the Tri-DSU prototype is only 232 g. The impact test for the Tri-DSU underloading was not performed.

7 Conclusions

In this paper, a new concept of discrete variable stiffness link is proposed for collaborative robots, leading to safe human–robot interaction. The basic principle is to change the cross-sectional area property of a hollow parallel beam structure. The concept allows discrete variations of stiffness using linear actuators. The design features of Tri-DSU are elaborated including eight stiffness configurations. Based on the superposition principle, an analytical

model for calculating the deflection and stiffness of the DSU segment by segment is established for the small/intermediate deflections. It is also generalized to a mathematical model of Tri-DSU, which implements to modularity and customization and is also applicable to multiple DSUs. Deflection and stiffness data of DSU with different parameters and configurations under various forces are collected through FEA simulations, mathematical analysis, and experiments. These data were compared and validated using the control variables method as well. Although the error of the analytical model becomes larger at higher stiffnesses, the results are still feasible in most cases satisfying the expected accuracy, which is less than 5%. The actual stiffness ratio of Tri-DSU can reach 31 in the experiment. Impact tests were also performed, and the minimum stiffness mode reduced the impact force by 67% compared to the maximum stiffness mode. Next, we will extend the concept to a commercial robotic arm design with practical human-robot impact testing and development.

Acknowledgment

This work was funded by the National Science Foundation (NSF) grant (Grant No. FRR-2131711, Award No. CIRA-2020-024) and the Purdue-Khalifa University collaboration project.

Conflict of Interest

There are no conflicts of interest.

Data Availability Statement

The datasets generated and supporting the findings of this article are obtainable from the corresponding author upon reasonable request.

References

- [1] Djuric, A. M., Rickli, J. L., and Urbanic, R. J., 2016, "A Framework for Collaborative Robot (CoBot) Integration in Advanced Manufacturing Systems,' SAE Int. J. Mater. Manuf., 9(2), pp. 457–464.
- [2] Aaltonen, I., Salmi, T., and Marstio, I., 2018, "Refining Levels of Collaboration to Support the Design and Evaluation of Human-Robot Interaction in the Manufacturing Industry," Procedia CIRP, 72, pp. 93-98.
- [3] Zhang, Y. J., Liu, L., Huang, N., Radwin, R., and Li, J., 2021, "From Manual Operation to Collaborative Robot Assembly: An Integrated Model of Productivity and Ergonomic Performance," IEEE Rob. Autom. Lett., 6(2), pp. 895-902.
- [4] Rozo, L., Calinon, S., Caldwell, D. G., Jiménez, P., and Torras, C., 2016, "Learning Physical Collaborative Robot Behaviors From Demonstrations," IEEE Trans. Rob., 32(3), pp. 513–527.
- [5] Gan, D., Tsagarakis, N. G., Dai, J. S., Caldwell, D. G., and Seneviratne, L., 2013, "Stiffness Design for a Spatial Three Degrees of Freedom Serial Compliant Manipulator Based on Impact Configuration Decomposition," ASME J. Mech. Rob., 5(1), p. 11002.
- [6] Ohta, P., Valle, L., King, J., Low, K., Yi, J., Atkeson, C. G., and Park, Y. L., 2018, Design of a Lightweight Soft Robotic Arm Using Pneumatic Artificial Muscles and Inflatable Sleeves," Soft Rob., 5(2), pp. 204-215.
- [7] Yang, H., Xu, M., Li, W., and Zhang, S., 2019, "Design and Implementation of a Soft Robotic Arm Driven by SMA Coils," IEEE Trans. Ind. Electron., 66(8), pp. 6108-6116.
- [8] Liang, X., Cheong, H., Sun, Y., Guo, J., Chui, C. K., and Yeow, C. H., 2018, "Design, Characterization, and Implementation of a Two-DOF Fabric-Based Soft Robotic Arm," IEEE Rob. Autom. Lett., 3(3), pp. 2702-2709.
- [9] Tonietti, G., Schiavi, R., and Bicchi, A., 2005, "Design and Control of a Variable Stiffness Actuator for Safe and Fast Physical Human/Robot Interaction,' Proceedings of the 2005 IEEE International Conference on Robotics and Automation, ICRA 2005, Barcelona, Spain, Apr. 18-22, pp. 526-531.

- [10] Liu, L., Leonhardt, S., Ngo, C., and Misgeld, B. J. E., 2020, Impedance-Controlled Variable Stiffness Actuator for Lower Limb Robot Applications," IEEE Trans. Autom. Sci. Eng., 17(2), pp. 991-1004.
- [11] Schiavi, R., Grioli, G., Sen, S., and Bicchi, A., 2008, "VSA-II: A Novel Prototype of Variable Stiffness Actuator for Safe and Performing Robots Interacting With Humans," Proceedings-IEEE International Conference on Robotics and Automation, Pasadena, CA, May 19-23, pp. 2171-2176.
- [12] Zhu, Y., Wu, Q., Chen, B., Xu, D., and Shao, Z., 2021, "Design and Evaluation of a Novel Torque-Controllable Variable Stiffness Actuator Reconfigurability," IEEE/ASME Trans. Mechatron., 27(1), pp. 292-303.
- [13] Choi, J., Hong, S., Lee, W., Kang, S., and Kim, M., 2011, "A Robot Joint With Variable Stiffness Using Leaf Springs," IEEE Trans. Rob., 27(2), pp. 229–238.
- [14] Xu, Y., Guo, K., Sun, J., and Li, J., 2021, "Design, Modeling and Control of a Reconfigurable Variable Stiffness Actuator," Mech. Syst. Signal Process., 160, p. 107883.
- [15] Hussain, I., Albalasie, A., Awad, M. I., Seneviratne, L., and Gan, D., 2018, "Modeling, Control, and Numerical Simulations of a Novel Binary-Controlled Variable Stiffness Actuator (BcVSA)," Front. Rob. AI, 5, p. 68
- [16] Awad, M. I., Gan, D., Hussain, I., Az-Zu'Bi, A., Stefanini, C., Khalaf, K., Zweiri, Y., Dias, J., and Seneviratne, L. D., 2018, "Design of a Novel Passive Binary-Controlled Variable Stiffness Joint (BpVSJ) Towards Passive Haptic Interface Application," IEEE Access, 6, pp. 63045–63057.
 [17] Morrison, T., and Su, H. J., 2020, "Stiffness Modeling of a Variable Stiffness
- Compliant Link," Mech. Mach. Theory, 153, p. 104021.
- [18] Morrison, T., Li, C., Pei, X., and Su, H. J., 2019, "A Novel Rotating Beam Link for Variable Stiffness Robotic Arms," Proceedings of the 2019 International Conference on Robotics and Automation (ICRA), Montreal, Canada, May 20-24, pp. 9387-9393.
- [19] Hu, R., Venkiteswaran, V., and Su, H. J., 2019, "A Variable Stiffness Robotic Arm Using Linearly Actuated Compliant Parallel Guided Mechanism," Mechanisms and Machine Science, Springer, Netherlands, pp. 33-40.
- [20] She, Y., Gu, Z., Song, S., Su, H. J., and Wang, J., 2021, "Design, Modeling, and Manufacturing of a Variable Lateral Stiffness Arm via Shape Morphing Mechanisms," ASME J. Mech. Rob., 13(3), p. 031020.
- [21] Chen, G., Zhang, Z., Kong, L., and Wang, H., 2020, "Analysis and Validation of a Flexible Planar Two Degrees-of-Freedom Parallel Manipulator with Structural Passive Compliance," ASME J. Mech. Rob., 12(1), pp. 1-10.
- [22] She, Y., Meng, D., Cui, J., and Su, H. J., 2017, "On the Impact Force of Human-Robot Interaction: Joint Compliance vs. Link Compliance,' Proceedings of the 2017 IEEE International Conference on Robotics and Automation (ICRA), Singapore, May 29-June 3, pp. 6718-6723.
- [23] Shintake, J., Cacucciolo, V., Floreano, D., and Shea, H., 2018, "Soft Robotic Grippers," Adv. Mater., 30(29), p. 1707035.
- [24] Zhou, L., Ren, L., Chen, Y., Niu, S., Han, Z., and Ren, L., 2021, "Bio-Inspired Soft Grippers Based on Impactive Gripping," Adv. Sci., 8(9), p. 2002017. [25] Pan, H., Chen, G., Kang, Y., and Wang, H., 2021, "Design and Kinematic
- Analysis of a Flexible-Link Parallel Mechanism With a Spatially Quasi-Translational End Effector," ASME J. Mech. Rob., **13**(1), pp. 1–12.
- [26] Hussain, I., Albalasie, A., Awad, M. I., and Gan, D., 2019, "Modeling, Identification, and Control of a Discrete Variable Stiffness Actuator (DVSA). Actuators, 8(3), p. 50.
- [27] Awad, M. I., Hussain, I., Gan, D., Azzu'bi, A., Stefanini, C., Khalaf, K., Zweiri, Y., Taha, T., Dias, J., and Seneviratne, L., 2019, "Passive Discrete Variable Stiffness Joint (PDVSJ-II): Modeling, Design, Characterization, and Testing Toward Passive Haptic Interface," ASME J. Mech. Rob., 11(1), p. 011005.
- [28] Fu, J., and Gan, D., 2021, "A Reconfigurable Variable-Stiffness Parallel Beam for Compliant Robotic Mechanisms Towards Safe Human Interaction," ASME International Design Engineering Technical Conferences and Computers and Information in Engineering Conference (IDETC-CIE2021), Virtual, online, Aug. 17-19.
- [29] Luo, Y., Liu, W., and Wu, L., 2015, "Analysis of the Displacement of Lumped Compliant Parallel-Guiding Mechanism Considering Parasitic Rotation and Deflection on the Guiding Plate and Rigid Beams," Mech. Mach. Theory, 91,
- Venkiteswaran, V. K., and Su, H. J., 2016, "Extension Effects in Compliant Joints and Pseudo-Rigid-Body Models," ASME J. Mech. Des., 138(9), p. 092302.
- [31] Awtar, S., and Sevincer, E., 2006, "Elastic Averaging in Flexure Mechanisms: A Multi-Beam Parallelogram Flexure Case-Study,", ASME 2006 International Design Engineering Technical Conferences and Computers and Information in Engineering Conference, Philadelphia, PA, Sept. 10-13, ASME International, pp. 251-257.
- [32] Awtar, S., Shimotsu, K., and Sen, S., 2010, "Elastic Averaging in Flexure Mechanisms: A Three-Beam Parallelogram Flexure Case Study," ASME J. Mech. Rob., 2(4), p. 041006.
- [33] Howell, L. L., Magleby, S. P., and Olsen, B. M., 2013, Handbook of Compliant Mechanisms, Wiley, New York.
- [34] Awtar, S., Slocum, A. H., and Sevincer, E., 2007, "Characteristics of Beam-Based Flexure Modules," ASME J. Mech. Des., 129(6), pp. 625-639.